

Spiral Structure of Cylindrical Batteries and its Importance in Modelling of Heat Transfer

Jiri Hvozda¹, Jan Bohacek¹, Alexander Vakhrushev², Ebrahim Karimi-Sibaki²

¹Heat Transfer and Fluid Flow Laboratory, Faculty of Mechanical Engineering
Brno University of Technology, Antoninska 548/1, 602 00 Brno, Czechia
Jiri.Hvozda@vut.cz; Jan.Bohacek@vut.cz

²Christian-Doppler Laboratory for Metallurgical Applications of Magneto hydrodynamics
Montanuniversitaet Leoben, Franz-Josef Strasse 18, 8700 Leoben, Austria
Alexander.vakhrushev@unileoben.ac.at; ebrahim.karimi-sibaki@unileoben.ac.at

Abstract - This study investigates the importance of considering the well-known spiral structure of cylindrical batteries in numerical models of heat transfer within the battery. Such models typically simplify the internal geometry by a concentric layout with electrodes and separators. This results in an effective orthotropic thermal conductivity with radial, tangential and axial components defined in a local cylindrical coordinate system. However, the actual spiral structure suggests radius-dependent thermal conductivity. Herein, several thermal simulations were performed, and thermal fields were compared with the commonly used cylindrical orthotropy and the more realistic spiral. The results show that the spiral does indeed have a negligible effect on the overall temperature distribution when realistically dense spirals are assumed, confirming the common assumption employed in the literature. Interestingly, none of the previous studies provide proof of the above assumption. Therefore, this paper can serve this purpose.

Keywords: battery thermal management systems, Li-Ion cylindrical batteries, orthotropic thermal conductivity, spiral structure

1. Introduction

Maintaining optimal temperature within Li-Ion cylindrical batteries is crucial for performance and safety. The temperature should remain within the 15–35 °C range, with temperature variations across the battery pack kept below 5 °C to avoid uneven degradation. Effective thermal management is vital to achieving this, and numerical simulations have emerged as indispensable tools for exploring and developing these systems [1–3].

A critical aspect of battery design is the internal structure, where cylindrical cells feature a spiral-wound arrangement of electrodes and separators. This spiral structure, visible in CT scans of batteries obtained by Finegan et al. [4], see Fig. 1, introduces complexities in heat transfer modelling. The most advanced thermal simulations incorporate the spiral's influence and electrochemical dynamics, such as concentration gradients and phase changes. While these high-fidelity models offer a detailed understanding of battery behaviour, they are computationally intensive and energy-demanding, limiting their use to specific applications [5–7].

Simpler models are often employed for routine simulations, especially at low discharging or charging rates. These models assume constant heat generation rates and neglect the internal spiral structure [8], in some cases even simplifying the thermal conductivity as isotropic [9]. At higher rates, more complex models incorporate the reversible and irreversible heat generation components. However, they still neglect the cell spiral structure, i.e. employ thermal conductivity tensor components as constant [10–12].

Although numerous studies assume orthotropic thermal conductivity with constant values in cylindrical coordinates, they often omit a justification for disregarding the spiral structure. This simplification is likely due to the ease of implementation in standard CFD software, which typically employs cylindrical orthotropic material properties that seem to address the problem at first glance. However, this approach is not entirely accurate and requires careful consideration to ensure that important factors, such as the spiral structure, are not overlooked. This paper fills that research gap by presenting

a series of numerical simulations that explicitly consider spiral geometry. Our results show that the spiral structure has a negligible impact on the overall thermal conductivity, thus validating the simplifications widely adopted in the literature.

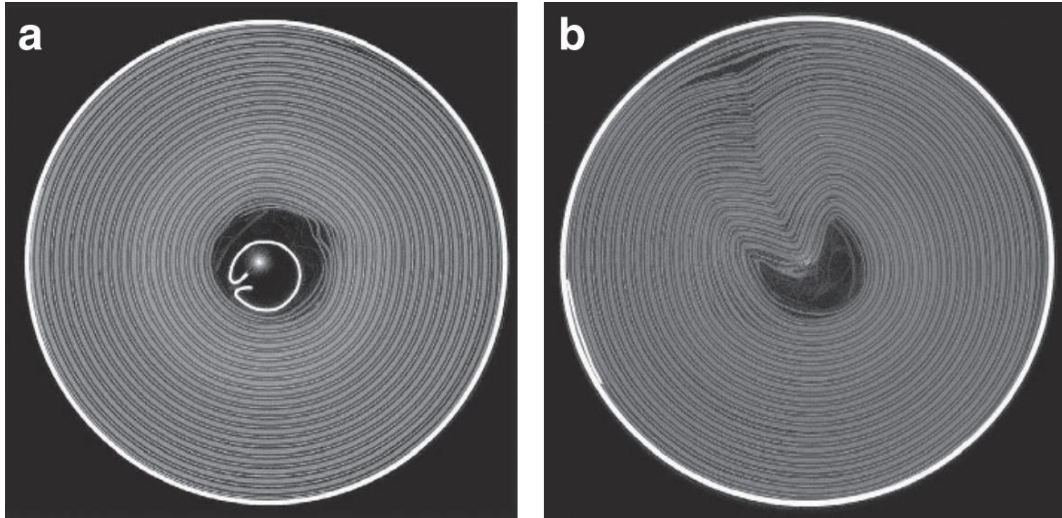


Fig. 1: CT images after venting in the XY plane comparing the spiral layered structure. 18650 cells (a) with and (b) without an internal support. Figure adapted from [4].

2. Methods

2.1. Governing equations and transformation from cylindrical to cartesian coordinates

The computational domain consists of a cylinder with a radius of 9 mm (r_o) representing an 18650 Li-Ion cell, the cross-sectional slice is displayed in Fig. 2. The case can be solved only in two-dimensional space x, y as heat transfer in the z -direction is trivial and is not connected with the primary goal of the present manuscript to test the influence of the spiral geometry on heat transfer. However, the equations and transformations are stated in three-dimensional space for their general usage. The Dirichlet boundary condition is set on the outer diameter of a cylinder with a constant wall temperature (T_{wall}). Steady state is assumed. This setting can simulate the case when a Li-Ion cell is discharging/charging at low current and immersed in a phase change material with melting point of T_{wall} .

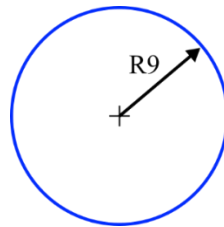


Fig. 2: Computational domain with displayed Dirichlet boundary condition (blue curve).

Governing equation follows as

$$0 = \nabla \cdot (K_{car} \nabla T) + S, \quad (1)$$

where S represents the heat generation rate. The thermal conductivity tensor K_{car} in the governing equation (1) must be implemented via transformation from local spiral (r, ϕ, z) to cartesian (x, y, z) coordinates as

$$K_{\text{car}} = \Sigma K_{\text{bat}} \Sigma^T, \text{ where} \quad (2)$$

$$\Sigma = \begin{bmatrix} \cos(\phi(r)) & -\sin(\phi(r)) & 0 \\ \sin(\phi(r)) & \cos(\phi(r)) & 0 \\ 0 & 0 & 1 \end{bmatrix} \text{ and} \quad (3)$$

$$K_{\text{bat}} = \begin{bmatrix} k_{\text{rad}} & 0 & 0 \\ 0 & k_{\text{tan}} & 0 \\ 0 & 0 & k_{\text{ax}} \end{bmatrix}. \quad (4)$$

In literature, the thermal conductivity of a cylindrical battery is often simplified by assuming concentric cylindrical layers of internal components, thus defining the thermal conductivity tensor in cylindrical coordinates – radial (k_{rad}), tangential (k_{tan}), and axial (k_{ax}), particular values are given in Table 1. The spiral structure will not influence the latter; the others must be changed concerning the radius to reflect the deviation (α) between tangential vectors of the circle and spiral in their intersection. The derivation of angle $\phi(r)$ is illustrated in Fig. 3 and is further described in the next section in detail.

Table 1: Thermal conductivity tensor components in the cylindrical coordinates of a cylindrical Li-Ion battery 18650 [13, 14].

Property	Value	Units
k_{rad}	0.2 or 2	$\text{W} \cdot \text{m}^{-1} \cdot \text{K}^{-1}$
$k_{\text{tan}} = k_{\text{ax}}$	30	$\text{W} \cdot \text{m}^{-1} \cdot \text{K}^{-1}$

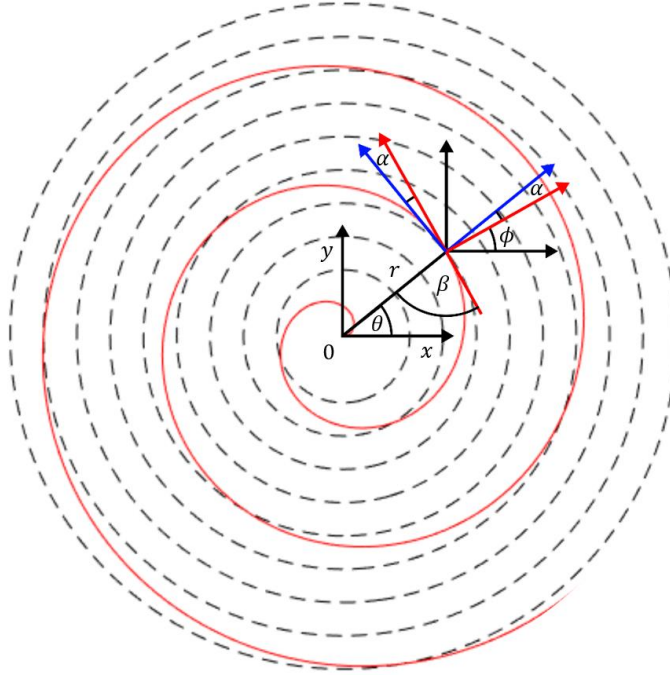


Fig. 3: Illustration of the intersection of a spiral with concentric circles with detail on angles used to describe the radius-dependent thermal conductivity. The black axis represents cartesian coordinates, and the blue and red axes correspond to local cylindrical and spiral thermal conductivity directions, respectively.

2.2. Description of the radius-dependent thermal conductivity in cylindrical coordinates

Based on the previous figure, it is straightforward to see that we have to find the angle α for every feasible value of the radius, i.e., in the interval of 0 and 9 mm. Then, for any point (r, θ) , the angle ϕ in eq. (3) is given as the difference of θ and α . Clearly, the sum of angles α and β is 90° . Let us proceed with finding the angle β . Note that, near the origin, the value β will be close to 0° , which is expected to increase and converge to 90° with increasing radius. In the following text, we will make the relations only in r, θ plane, as the spiral structure does not influence the behaviour in z direction. The circle with radius R can be written as

$$r = R \quad (5)$$

and the spiral follows as

$$r = b\theta, \quad (6)$$

where b defines the gap between the spiral layers. The angle β can be obtained from the formula of the angle between a tangential of the spiral and radius vector as

$$\tan \beta = r \frac{d\theta}{dr}. \quad (7)$$

Further, derivation of equation (6) by θ and substituting term $d\theta/dr$ into (7) yields

$$\tan \beta = \frac{r}{b} \Rightarrow \beta = \arctan \frac{r}{b}. \quad (8)$$

And, thus

$$\phi = \theta - \alpha = \theta - 90^\circ + \arctan \frac{r}{b}. \quad (9)$$

The resulting angle α is shown in Fig. 4 a), for four different b . In practice, actual values of b are somewhat lower than $r_0/(20\pi)$ m, i.e. the spiral has more than eleven layers. For these cases, it can be seen that if the radius is higher than 1 mm, the angle α is lower than 8° . Hence, the difference between the constant and variable conductivity (based on the spiral structure) is minor, and no significant temperature difference is expected for cases with varying thermal conductivity with radius.

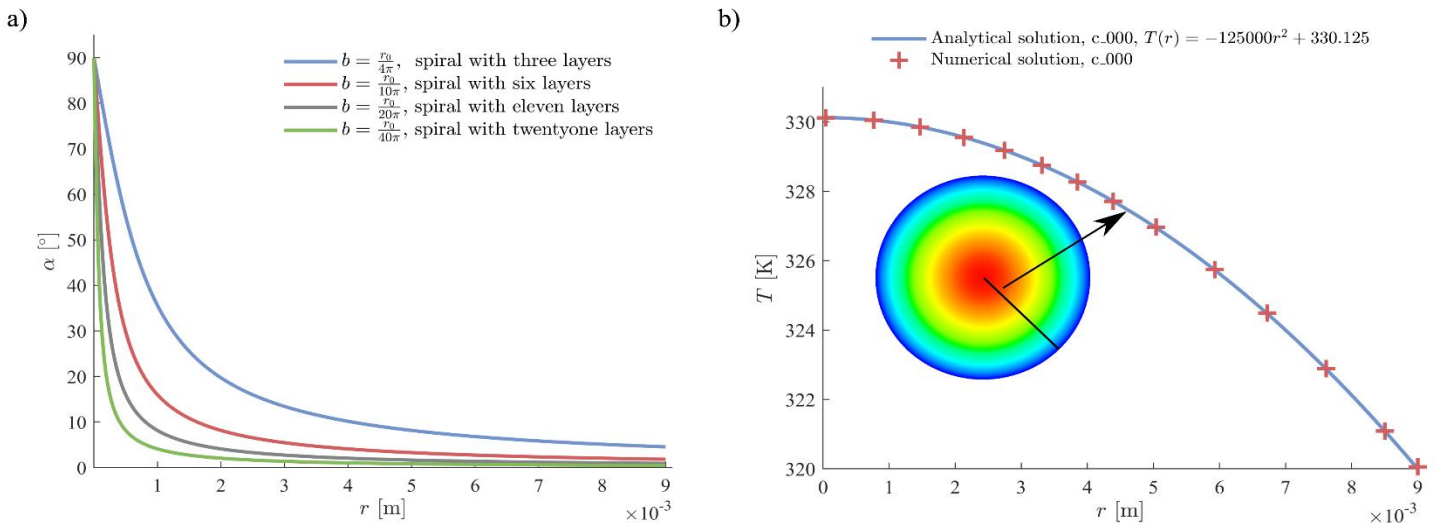


Fig. 4: a) Value of angle α for various b along the radius inside a computational domain, b) analytical and numerical temperature profile along radius for case c_00 with a detail on the temperature distribution inside the computational domain.

2.3. Plan of the simulations

Simulations were performed in ANSYS Fluent 2024 R1. Several simulations were conducted for cases with constant thermal conductivities and varying conductivity with respect to the radius described in the previous section for several setups of coefficient b . Their settings are shown in Table 2.

Table 2: Plan of the simulations.

case	$b \cdot \frac{2\pi}{r_0}$ [-]	k_{rad} $\text{W} \cdot \text{m}^{-1} \cdot \text{K}^{-1}$	k_{tan} $\text{W} \cdot \text{m}^{-1} \cdot \text{K}^{-1}$	S $\text{kW} \cdot \text{m}^{-3}$	T_{wall} K
c_000	–	0.2	30	100	320
s_020	20	0.2	30	100	320
s_010	10	0.2	30	100	320
s_005	5	0.2	30	100	320
s_002	2	0.2	30	100	320
c_100	–	2	30	100	320
s_120	20	2	30	100	320
s_110	10	2	30	100	320
s_105	5	2	30	100	320
s_102	2	2	30	100	320

3. Results

For the cases c_000 and c_100, i.e. one-dimensional heat conduction in steady state regime, equation (1) can be rewritten into the form

$$0 = \frac{\partial^2 T}{\partial r^2} + \frac{1}{r} \frac{\partial T}{\partial r} + \frac{S}{k_{\text{rad}}}. \quad (11)$$

By standard approach, it can be analytically found the particular solution of temperature distribution along the radius inside the computational domain as

$$T(r) = \frac{S}{4k_{\text{rad}}}(r_0 - r^2) + T_{\text{wall}}. \quad (12)$$

The comparison of analytical and numerical solutions of case c_000 are displayed in Fig 4 b). As can be seen, the numerical solution follows the correct analytical solution; thus, the numerical approach is assumed to be validated. The simulation results for all cases are shown in Table 3. It can be seen that the change of b influences the maximal temperature inside the battery significantly. The absolute error is up to 9.65 K, but the relative error is lower than 2.92 %. A significant difference can be observed for the maximal temperature spread, especially for very low values of b . The relative error goes up to almost 95.45 %. A low value of b causes high conductivity along the sparse spiral that effectively removes heat to the sides of the battery.

Table 3: Results of the simulations.

case	T_{\max} K	$T_{\max,s-c}$ K	ε_{\max} %	ΔT_{\max} K	$\Delta T_{\max,s-c}$ K	$\varepsilon_{\Delta\max}$ %
c_000	330.12	–	–	10.01	–	–
s_020	330.12	0.00	0.00	10.00	0.00	0.02
s_010	330.12	0.00	0.00	10.00	0.00	0.02
s_005	323.73	6.39	1.93	3.67	6.34	63.36
s_002	320.46	9.65	2.92	0.46	9.55	95.45
c_100	321.01	–	–	1.00	–	–
s_120	321.01	0.00	0.00	1.00	0.00	0.00
s_110	321.01	0.00	0.00	1.00	0.00	0.00
s_105	320.82	0.19	0.06	0.81	0.19	1.88
s_102	320.32	0.69	0.21	0.32	0.68	6.81

4. Conclusion

Based on the results of the difference between spiral and circular thermal conductivity, it can be said that it is not required to use the spiral structure in the numerical model as for real cases ($b > 10 \cdot 2\pi/r_o$) no difference can be observed at all in temperature fields. The explanation is that tangential vectors of circles and a spiral at intersection points have almost identical directions for points further than 1 mm from the origin. On the other hand, for very sparse spirals, a significant error occurs (up to 10 K) due to the very effective heat removal along the spiral to the outside of the battery. Indeed, the thermal conductivity tensor can be assumed to have constant components – radial, tangential and axial, in standard simulations.

Acknowledgements

This work was supported by projects "The Energy Conversion and Storage", funded as project No. CZ.02.01.01/00/22_008/0004617 by Programme Johannes Amos Comenius, call Excellent Research and "Hollow Fiber Exchangers with Reduced Permeability for Smart Cities", funded as project No. 8I24002 by Programme EIG CONCERT Ministry of Education, Youth and Sports.

References

- [1] F. Herrmann, F. Rothfuss, *Advances in Battery Technologies for Electric Vehicles*, Sawston: Woodhead Publishing, 2015.
- [2] Q. L. Yue, C. X. He, M. C. Wu, T. S. Zhao, "Advances in thermal management systems for next-generation power batteries," *International Journal of Heat and Mass Transfer*, vol. 181, p. 121853, 2021.
- [3] A. Gharehghani, M. Rabiei, S. Mehranfar, S. Saeedipour, A. M. Andwari, A. García, C. M. Reche, "Progress in battery thermal management systems technologies for electric vehicles," *Renewable and Sustainable Energy Reviews*, vol. 202, p. 114654, 2024.
- [4] D. P. Finegan, M. Scheel, J. B. Robinson, B. T., I. Hunt, T. J. Mason, J. Millichamp, M. Di Michiel, G. J. Offer, G. Hinds, D. J. L. Brett, P. R. Shearing, "In-operando high-speed tomography of lithium-ion batteries during thermal runaway," *Nature Communications*, vol. 6, no. 1, Apr. 2015.
- [5] Q. Wu, L. Yang, N. Li, Y. Chen, Q. Wang, W. Song, X. Feng, Y. Wei, H. Chen, "Temperature field evolution of cylindrical battery: In-situ visualizing experiments and high fidelity internal morphology simulations," *Journal of Power Sources*, vol. 499, p. 229910, 2021.
- [6] V. Ramadesigan, P. W. C. Northrop, S. De, S. Santhanagopalan, R. D. Braatz, V. R. Subramanian, "Modeling and simulation of lithium-ion batteries from a systems engineering perspective," *Journal of the Electrochemical Society*, vol. 159, no. 3, pp. R31-R45, 2012.
- [7] H. Kim, J. H. Choi, K. Lee, "A numerical study of the effects of cell formats on the cycle life of lithium ion batteries," *Journal of The Electrochemical Society*, vol. 166, no. 10, pp. A1769-A1779, 2019.
- [8] X. Qian, D. Xuan, X. Zhao, Z. Shi, "Heat dissipation optimization of lithium-ion battery pack based on neural networks," *Applied Thermal Engineering*, vol. 162, p. 114289, 2019.
- [9] S. A. Khateeb, S. Amiruddin, M. Farid, J. R. Selman, S. Al-Hallaj, "Thermal management of Li-ion battery with phase change material for electric scooters: experimental validation," *Journal of Power Sources*, vol. 142, no. 1-2, pp. 345-353, 2005.
- [10] C. R. Pals, J. Newman, "Thermal modeling of the lithium/polymer battery: I. Discharge behavior of a single cell," *Journal of the Electrochemical Society*, vol. 142, no. 10, pp. 3274-3280, 1995.
- [11] J. E. Jiaqiang, M. Yue, J. Chen, H. Zhu, Y. Deng, Y. Zhu, F. Zhang, M. Wen, B. Zhang, S. Kang, "Effects of the different air cooling strategies on cooling performance of a lithium-ion battery module with baffle," *Applied Thermal Engineering*, vol. 144, pp. 231-241, 2018.
- [12] A. Kaabinejadian, H. A. Ahmadi, M. Moghimi, "Investigation of porous media effects on lithium-ion battery thermal management," *Journal of Thermal Analysis and Calorimetry*, vol. 141, pp. 1619-1633, 2020.
- [13] Y. Jiang, J. Huang, P. Xu, P. Wang, "Axial and radial thermal conductivity measurement of 18650 Lithium-ion battery," *Journal of Energy Storage*, vol. 72, p. 108516, Nov. 2023.
- [14] S. J. Drake, D. A. Wetz, J. K. Ostanek, S. P. Miller, J. M. Heinzl, A. Jain, "Measurement of anisotropic thermophysical properties of cylindrical Li-ion cells," *Journal of Power Sources*, vol. 252, pp. 298-304, Apr. 2014.